van der Waals Epitaxy of GaSe/Graphene Heterostructure: Electronic and Interfacial Properties

Zeineb Ben Aziza[1], Hugo Henck[1], Debora Pierucci[1], Mathieu G. Silly[2], Emmanuel Lhuillier[3, 4], Gilles Patriarche[1], Fausto Sirotti[2], Mahmoud Eddrief[3, 4] and Abdelkarim Ouerghi[1]

[1] Laboratoire de Photonique et de Nanostructures (CNRS-LPN), Route de Nozay, 91460 Marcoussis, France
[2] Synchrotron-SOLEIL, Saint-Aubin, BP48, F91192 Gif sur Yvette Cedex, France
[3] Sorbonne Universités, UPMC Univ. Paris 06, UMR 7588, INSP, F-75005 Paris, France
[4] CNRS, UMR 7588, Institut des NanoSciences de Paris (INSP), F-75005 Paris, France

Abstract: Stacking two-dimensional (2D) crystals in so-called van der Waals heterostructures, like the combination of 2D-layered GaSe and graphene, provides the ability to obtain hybrid systems which are excellent candidates to design novel nanoelectronic and optoelectronic devices. Here, we report the electronic and structural properties of the direct large scale growth of few GaSe layers by Molecular beam Epitaxy (MBE) on graphene/SiC. RHEED images showed sharp streaky features indicative of atomically flat GaSe films grown via a van der Waals epitaxy (vdW). Micro-Raman spectroscopy showed that, after a van der Waals hetero-interface formation, the Raman signature of pristine graphene is preserved. However, the GaSe growth tuned the electronic properties of graphene by shifting the Dirac point by about 80 meV toward lower binding energies with respect to the π-band of pristine graphene, attesting an electron transfer from graphene to GaSe. ARPES measurements showed that the maximum of the valence band of few layers GaSe are located at the Γ point at a binding energy of about -0.73 eV relative to the Fermi level (p-type doping). From the ARPES measurements, a hole effective mass defined along the ΓM direction and equal to about $m^*/m_0 = -1.1$ was determined. By coupling the ARPES data with XPS measurements, the Schottky interface barrier height was estimated to be 1.2eV. These findings about interlayer interactions and electronic structure of 2D heterostructure represent a key issue for the new devices concepts.

KEYWORDS: Van der Waals heterostructures – GaSe/graphene – Molecular Beam Epitaxy – RHEED – XPS/ARPES – Band structure –Raman spectroscopy – Charge transfer.

Graphene is a single layer of carbon atoms arranged in honeycomb lattice. Despite graphene high carrier mobility, the absence of a band gap limits its application in the field of optoelectronics[1]. From here comes the importance of exploring the interaction with other 2D materials, in particular with the family of artificially structured materials such as transition metal dichalcogenide (TMDCs like MoS_2) and semiconducting metal monochalcogenide (GaSe, InSe)[2,3,4,5]. The stacking of layered materials on top of each other permits the creation of novel functional materials and promises tunable optoelectronic properties for future devices with improved functionalities [1,6,7].

GaSe is a van der Waals layered material, possessing a strong in-plane *vs* out-of-plane electronic conduction anisotropy which results from highly anisotropic bonding forces[8]. The atoms in unit of atomic tetra-layer (TL) *i.e.* Se-Ga-Se-Ga: TL, have strong bonds and all bonds are saturated on TL surface. Moreover, the 2D-TLs are stacked in the out-of-plane direction *via* weak inter-TLs van der Waals interactions. The layered hexagonal GaSe was chosen to be the optical active material because of its high photoresponsivity (2.8 AW^{-1}) and high external quantum efficiency (≈1300%) that were recently demonstrated [5]. As grown GaSe is a p-type semiconductor, this p-type character provides a major property because in the 2D family most of the TMDCs are n-type[9]. Moreover, GaSe has a direct bandgap of about 2.1 eV, for a number of layers greater than seven[10–12]. The two minima of the conduction band can both be populated by photoexcited carriers. The radiative recombination, associated with the direct and the indirect gaps, may occur simultaneously. This makes GaSe a promising material for optoelectronic applications[5,13,14]. The GaSe based optoelectronic devices cannot only be used as photodetectors and THz source generator[15], but also for the nonlinear optical applications[16] due to its large nonlinear optical coefficient (54 pmV^{-1}). Various methods have been reported to grow GaSe thin films, including chemical vapor deposition[17], pulsed laser deposition[18], and molecular beam epitaxy[19, 20] (MBE). Apart from early pioneering works [19,20] there are a few works on the MBE growth of atomically thin epitaxial GaSe on insulating substrates and they are mainly focusing on the electronic properties. Indeed, they focus on the structural properties, and on the optical emission properties of epitaxial single and few-layer GaSe grown on sapphire and silicon by MBE [4,21].

Therefore, we demonstrate in this work a novel approach to assemble GaSe with epitaxial graphene/SiC; this paves the way for the realization of a well-ordered GaSe/graphene based heterostructure. The synthesis of multilayer intrinsic p-type GaSe is obtained by molecular beam epitaxy (MBE) on n-type epitaxial graphene on SiC(0001). This approach

enables the growth of large area vertical p-n junction van der Waals heterostructure. Compared to the conventional heterojunctions of 3D materials, this 2D heterojunction has several advantages. First, the combination of epitaxial graphene/SiC (chemical inert surface and massless-Dirac conduction) with the MBE growth of GaSe (with intrinsic gap) allows a full control at the atomic scale of the vertical thickness of the heterostructure with an almost perfect interface. Moreover, the absence of the Fermi-level pinning at the atomically sharp heterointerfaces, offers a unique opportunity to realize devices with gate-tunable characteristics [22]. This study is focused on understanding the electronic structure of GaSe as well as the interlayer coupling between GaSe and graphene. The understanding of the interface physics at the atomic scale is a challenging issue for the design of new devices with more functionality. In particular, RHEED was employed to control both the in-plane axis epitaxy alignment of GaSe film with respect to the graphene substrate and to control the crystalline quality during the growth. Micro-Raman spectroscopy was conducted to explore the vibration frequencies of phonons corresponding to the characteristic vibrational modes of layered GaSe on epitaxial graphene. After GaSe/Graphene heterointerface formation, the shifts observed in the Raman spectra of graphene layer reveal that a charge transfer has occurred between the p doped few layers GaSe and the n doped graphene. ARPES was used to investigate the electronic properties of GaSe *i.e.* the GaSe band structure and also the position of the valence band maximum relative to the Fermi level. This information coupled with the work function measurements by high resolution x-ray photoemission spectroscopy (HR-XPS) allows determining the Schottky barrier height (SBH) at the GaSe/graphene heterostrucutre.

Results and discussions:

Thermal decomposition of SiC(0001) can be used to produce large graphene films with a long-range order and high electron mobility[23]. Monolayer, bilayer, and few-layer graphene on SiC are obtained by tuning different experimental parameters (temperature, annealing times, and thickness of the SiC substrate)[24]. The graphene used in this study was obtained by annealing 6H-SiC(0001) at 1550 °C in an Ar atmosphere (see methods). The sample was divided into two parts, the first is considered as a reference and will be named hereafter “pristine graphene”, and the second has been used for the growth of few layers GaSe. The details of the growth are outlined in methods section.

Layered GaSe has planar TL character with in-plane hexagonal lattice and multi-stacked TLs along the c-axis with a relatively weak interlayer coupling, enabling its isolation down to a single TL. Each atomic TL consists of four covalent bonds, with an in-plane lattice constant of 0.37 nm and a TL thickness of about 0.8 nm[25,26]. Schematics of GaSe/graphene hybrid system and the top view of the in-plane GaSe hexagonal crystal structure are shown in Figure 1(a). Figure 1(b) presents the RHEED image of pristine graphene/SiC. Figure 1(c) show the RHEED pattern of GaSe film deposited on epitaxial graphene. Graphene and GaSe display in-plane hexagonal symmetry with hexagon's sizes of a_{GaSe} =0.374 nm and of $a_{Graphene}$ = 0.247 nm. The appearance of the sharp elongated streaks in the RHEED patterns, in early stage of the growth of GaSe film until the end of the growth process, suggests a well-crystallized order and flat surface of GaSe epilayer. Figure 1(c) shows that the presence of two streaky-lines pattern (two periods indicated by red and blue arrows) and they are correlated with in-plane <1-100>-axis and <11-20>-axis of in-plane hexagonal GaSe. Two main orientations of the GaSe domains are observed from the nucleation phase (in the early first GaSe TL coverage regime) as we illustrate in a scheme drawing in Figure 1(d) with aligned triangular GaSe islands on graphene (with a 180°-twinned ones) together with their ~ 30° rotated islands apart. From RHEED images in Figure 1(b) and (c), we extracted the large lattice mismatch between GaSe and graphene that is equal to -12.6% for GaSe domain aligned with the underlying graphene and of + 51.4% for the 30° rotated domains.

This hybrid 2D-layered material/Graphene interface is often understood to be formed through van der Waals forces[20] and does not involve covalent bonding[9]. Often two in-plane domain orientations of 2D materials growth on graphene are mentioned, particularly by molecular beam method, without understanding if its origin is related to the kinetics of the growth or to the presence of defects on the surface of graphene (even for very low density)[27]. One additional advantage of graphene as a supporting substrate for GaSe is to promote the GaSe growth at lower substrate temperatures (200 - 250 °C). The ability to decrease the growth temperature of such 2D materials represents a big advantage for large scale device manufacturing in particular for applications where heterogeneous integration with graphene devices is required.

To study the interface structure and chemical compositions at the local scale of the GaSe/graphene heterostructures, we have carried out scanning transmission electron microscopy (STEM) and selective area electron diffraction (SAED) studies. Figure 2(a) shows a typical low magnification STEM image of 2D GaSe/graphene. The STEM image indicating the 2D layered crystals are preferentially oriented in the c-axis direction. This image indicates

that the 2D GaSe film is structurally uniform and highly crystalline. Figure 2(b) shows a typical STEM image a high resolution of the GaSe with clear hexagonal lattice structure along the c axis. The lattice spacing is measured as 0.4 nm, as expected for the hexagonal GaSe along the (0001) axis (insert figure 2(b)). The interlayer separation between the graphene underlayer and the GaSe was about 0.33 nm. This interlayer distance was in agreement with that for vdW heterostructure[28]. The composition of the GaSe layer was studied by Energy Dispersive X-ray Spectroscopy (EDX) mapping as shown in figure 2(c) and 2(d). The specially resolved EDX elemental mapping of the Ga and Se show relatively uniform distribution, indicating composition uniformity across the films. The EDX images demonstrate a high crystalline and continuous film of GaSe, in which the Ga and Se atomic range could be identified. The results clearly show the presence of a sharp interface without inter-diffusion between GaSe and graphene layer. Interestingly, the GaSe layer exhibits a homogenous chemical composition. The EDX spectra revealed that the 2D film consist of Ga and Se with an atomic ratio of 1:1.

We then used micro-Raman spectroscopy to probe the effects of the presence of GaSe on the vibrational and electronic properties of graphene. A typical Raman spectrum of bulk GaSe consists of characteristic peaks for the A^1_{1g} mode, E^1_{2g} mode, E^2_{1g} mode, and A^2_{1g} mode. The two A_{1g} modes correspond to the out-of-plane vibrational mode of the Se-Ga-Ga-Se lattice, while E_{1g} and E_{2g} are associated with the in-plane vibrational mode. Figure 3(a) shows the Raman spectra performed with a 532 nm laser wavelength in different positions of the sample. We notice the presence of three of GaSe characteristic peaks, where the most prominent Raman mode corresponds to the A^1_{1g} mode at 132 cm^{-1}. The Raman vibrational modes at E^1_{2g} at 206 cm^{-1}, and A^2_{1g} at 307cm^{-1} are weak with small peak intensities. Moreover, the E^2_{1g} Raman peak around 260 cm^{-1} is almost due to the reduction in the scattering centers for E_{1g} mode so that the Raman scattering for this mode becomes less effective [29,2]. These spectra confirm what was reported for decreasing peaks intensities with reducing layer thickness [30]. The number of peaks together with their respective intensities indicate that the grown GaSe film is multi-layered [21,31,3].

Figure 3(b) shows a representative Raman spectrum of GaSe/graphene in the wavelength range 1300-2800 cm^{-1}. Numerous spectra were acquired in different areas of the substrate in order to check the uniformity of the signal. These spectra exhibit the three main peaks expected for graphene samples: i) D band at 1355 cm^{-1}, ii) G band at 1595 cm^{-1} and iii) 2D band at 2705 cm^{-1}. The D peak is barely visible, indicating the high quality of pristine graphene. Moreover, the

intensity of this peak does not increase after the GaSe growth suggesting that the formation of the heterostructure did not induce defects in the graphene underlayer.

Since the 2D and G bands positions are strongly dependent on the charge carrier concentration; they are used as probe of the graphene doping level. In order to better resolve the G peak of our spectra a background subtraction was done *i.e.* the spectrum of the SiC substrate (before the graphitization process) was used as reference and subtracted from the graphene one. In our GaSe/graphene heterostructure, we observe a clear upshift of the 2D mode. Since in our Raman measurements the spectra were taken at room temperature and the laser power was low enough to avoid the influence of laser heating, the observed 2D band upshift does not originate from strain induced by temperature gradients. Hence, this upshift of the 2D peak indicates a decrease in the electron concentration in graphene *i.e* a decrease of the n-type doping of epitaxial graphene on SiC induced by the GaSe layers. This phenomenon indicates that when graphene contacts GaSe, a dipole layer is formed at the interface due to electron transfer from graphene to GaSe [32].

Furthermore, the G peak presents a downshift of about 3 cm^{-1} in the case of GaSe on graphene which can give us a more quantitative estimation of the hole doping. Based on the formula $\omega_G - 1580 = |E_F| \times 42\ cm^{-1}eV^{-1}$ linearly linking the G peak energy to the Fermi level [33–35], we estimate a decrease in the graphene Fermi level of about 80 ±5 meV attesting a decrease in the n-type doping of graphene. From the corresponding Fermi energies, we calculate the variation in the doping level of graphene thanks to the following relation between the doping density N and the Fermi level E_F: $|E_F| = \hbar v_F \cdot \sqrt{\pi |N|}$. For a Fermi velocity equal to $v_F = 1.1 \times 10^6\ m/s$ [36,37], we obtain an electron doping density for the pristine graphene $|N| \sim 1.6 \times 10^{13}\ cm^{-2}$ which decreased to $|N| \sim 1.1 \times 10^{13}\ cm^{-2}$ for the GaSe/graphene heterostructure. Therefore, the hole doping density induced to graphene is found to be equivalent to $\Delta|N| \sim 5 \times 10^{12}\ cm^{-2}$. Similar behavior was also observed with 2D CdSe nanoplatelets and epitaxial graphene, where a much larger electron transfer from graphene to CdSe was demonstrated so that graphene switched from n to p type character[38]. It is worth noting that the alteration of the G mode Raman frequencies caused by eventual strain could not be completely excluded but in this case the shift of the G peak should be in the same direction as the shift of the 2D peak[39] i.e. a shift toward higher frequencies. To calculate the charge transfer, we considered the downshift of the G peak; it could be underestimated in presence of strain[40].

HR-XPS measurements were carried out to uncover the electronic properties and ensure the stoichiometric of the GaSe/graphene heterostructure. The XPS spectra recorded under surface sensitive conditions hν = 60 eV for Ga *3d* and hν = 100 eV for Se 3d are shown in Figure 4(a) and (b), respectively. The spectra were analyzed using the curve fitting procedure described in Methods. The binding energies (BEs) of the Ga $3d_{5/2}$ and Se $3d_{5/2}$ core levels are 19.8 eV and 54.7 eV, respectively[41]. These values are in good agreement with others reported on thin-film and bulk single-crystal [19,42]. In both spectra, there is no signature of other bonds[43] (i.e. oxygen or carbon), indicating that the GaSe crystal are not contaminated. The work function of pristine graphene and few TL GaSe were also determined via the measurement of the low energy cut-off of the secondary electron (SE) energy distribution curve obtained by XPS measurements at a photon energy of hν = 100 eV (Figure 4(c)), see method. A value of 4.30 eV ±0.05 eV is found for the pristine graphene, and 4.70 ± 0.05 eV with the few TL GaSe. We used angle-resolved photo electron spectroscopy (ARPES) to study the band structure of the GaSe films on epitaxial graphene. Figure 5(a) illustrates the valence band structure of few TL GaSe around the Γ point of the first Brillouin zone (BZ) using an excitation energy hν = 60 eV. In order to get better clarity of the bandstructure, the second derivative of the photoelectron intensity as a function of energy and k-momentum, is shown in Figure 5(b). The zero binding energy (i.e, the Fermi level) is taken at the leading edge of a clean metal surface in electrical contact with the heterostructure.

In Figure 5(c) the measured band structure was compared with theoretical calculation of bulk GaSe of X. Li et al.[31]. Due to the fact that the sample is formed of two GaSe domains at 0° and 30°, we superimposed to the ARPES spectrum the dispersion along the ΓM direction (Figure 5(c)) and the ΓK direction (Figure S1) of the bulk GaSe Brillouin zone (BZ). The measured band structure along the ΓM direction presents a good agreement with the theoretical calculation as shown in Figure 5(c). The dispersion along the ΓK direction illustrated in Figure S1 shows that some of the bands along this direction are also visible and results from the presence of two GaSe domains. This result proves the high quality of the grown GaSe on top of graphene/SiC as well as the unaffected band structure of GaSe within our van der Waals heterostructure[8]. In particular as expected for a bulk GaSe, the maximum of the valence band (VBM) is located at the Γ point, ensuring that the number of TL GaSe presents on the sample are greater than seven[31]. In fact as the number of layer decrease (less than 7 TL) the VBM splits in a symmetric way along the Γ point, and the band gap pass from direct to indirect, demonstrating an opposite behavior compared with TMDCs[44,45] .

We have also determined the effective mass of the hole close to the Γ point of the BZ along the ΓM high symmetry directions. The experimental dispersion has been fitted with a parabolic model $E(k) = E_0 + \frac{\hbar^2}{2m^*} k^2$ where m* is the effective electron mass and ħ is the reduced Planck constant. We found that the hole effective mass at the Γ point is about m^*/m_0 = -1.1±0.1, see Figure 5(d) where the dispersion fitting used to calculate the effective mass is illustrated. One can notice that this mass is close to m_0 which implies that the GaSe band is poorly dispersive suggesting a very limited mixing of the valence band[46]. Furthermore, this calculated effective mass obtained at room temperature along the ΓM direction is nearly twice the in-plane mass calculated for GaSe at low temperature (at 10K)[11]. This difference could be explained by the fact that the effective mass is anisotropic and hence varies greatly with the measurement direction.

According to the above values from XPS and APRES measurements, we are able to figure out the band offsets resulting from the junction formation. In fact, one of the most determining properties of a metal-semiconductor interface is its Schottky-barrier height (SBH), which is a measure of the mismatch of the energy levels for the majority of carriers across the metal-semiconductor interface. In the case of p-doped few TL GaSe /n-doped graphene heterostucture, the lack of dangling bonds on both surfaces implies the absence of surface states. Moreover, no bonds are present at the interface between the two materials, i.e. the heterostructure is held only by van der Waals interactions. Alike a standard metal-semiconductor interface, the particular properties of these vdW heterostructure ensure the formation of a quasi-ideal (semi) metal – semiconductor interface with a behavior approaching the Schottky limit where the SBH is given by the difference between the metal work function (ϕ_m) and the electron affinity (χ) of the semiconductor[47]. In our case the pristine graphene is n-doped and presents a work function of 4.30 eV. The few TL GaSe present a p-type doping and a measured work function of 4.70 eV (i.e. an electron affinity of 3.4 eV[42] considering a band gap of 2.1 eV[48–50]). At thermal equilibrium the Fermi level in the two materials must be aligned. The charge flow from the graphene to the GaSe, as confirmed by the Raman measurements, leads to the formation of a dipole layer at the interface. In the GaSe an accumulation region is formed followed by a downwards band bending.

Then the SBH formed at the interface is given by:

$$SBH = E_g - (\phi_m - \chi) = 1.2\ eV$$

Based on this calculated value, the band alignment diagram of the GaSe/graphene heterostructure is derived and shown in Figure 6. The measurement of this SBH is of fundamental importance to the successful design of any semiconductor device as it controls the electronic transport across the metal-semiconductor interface. In particular, thanks to the extreme low reactivity of these hexagonal two dimensional layered structures, we managed to obtain a p-n junction between a (semi)-metal and a semiconductor in which the interface operates close to the Schottky limit. Moreover, the tunability of graphene work function, e.g. by electrostatic doping[51] can be exploited to adjust the graphene Fermi level to the GaSe conduction band minimum to reduce or completely remove this Schottky barrier at the interface. Concerning this point, the MBE growth process of the GaSe on graphene ensures a high purity growth and a high control of the number of TL allowing to easily change the thickness of the heterostructure from few TL to one TL. This is a huge step forward in the all 2D metal-semiconductor junction engineering, because by reducing the GaSe thickness to one TL we are able in principle to induce a vanishing of the depletion region and a total collapse of the Schottky barrier creating an Ohmic contact.

Another highly interesting aspect of our method was the p intrinsic doping of the GaSe few TL on n doped graphene. Theoretical studies have predicted that the band gap of the GaSe may be widely tuned by varying the numbers of layer in the crystal or by inducing mechanical strain[52,31]. The GaSe/graphene/SiC structure is of particular interest because the stepped surface of graphene/SiC substrate is expected to produce a periodic strain or auto-organisation of monolayer/bilayer graphene[53] that is strictly mechanical in nature, as well as a charge modulation beneath the GaSe. This modulation is a result of confinement, with a significant one-dimensional (1D) or two-dimensional (2D) lateral potential modulation induced by the nanofacet of the graphene substrate[54]. These effects can be exploited to induce tunable band gaps in GaSe electronic structure with the hope of making practical 2D materials devices.

Conclusions:

In summary, we demonstrate the molecular beam epitaxial growth of hybrid graphene/SiC (0001) heterostructure via van der-Waals epitaxy process. Even though the lattice mismatch between GaSe and graphene is at least 12.6 %, the heterostructure is commensurate, epitaxial growth is reached with well-defined crystalline GaSe films in spite of a two in-plane GaSe rotated domains. GaSe induces a decrease in the charge density of the graphene underlayer. ARPES measurement reveals the GaSe electronic structure: the Fermi level position indicates

a p-type doping and theVBM is located at the Γ point, as expected for a bulk-like GaSe band structure (i.e. number of TL greater than seven). Combining ARPES results with work function measurements, the Schottky barrier height at the GaSe/graphene of the heterostructure was determined. This successful synthesis of few layered GaSe on large area epitaxial graphene substrate can pave the way to broaden the use of 2D GaSe crystals as excellent candidates for optoelectronic applications with high photoresponse and FET characteristics.

Acknowledgements: This work was supported by the H2DH grants. We acknowledge support from GANEX (Grant No. ANR-11-LABX-0014) and Labex "Nanosaclay (Grant No. ANR-10-LABX-0035)". GANEX belongs to the public funded Investissements d'Avenir program managed by the French National Research Agency.

Supporting Information:

Section I: Sample preparation and characterization methods. Section II: Comparison between the measured band structure and the theoretical calculation of bulk GaSe along the ΓK direction (Figure S1). This materials is available free of charge via the Internet at http://pubs.acs.org.

Competing financial interests: The authors declare no competing financial interests.

Figure captions:

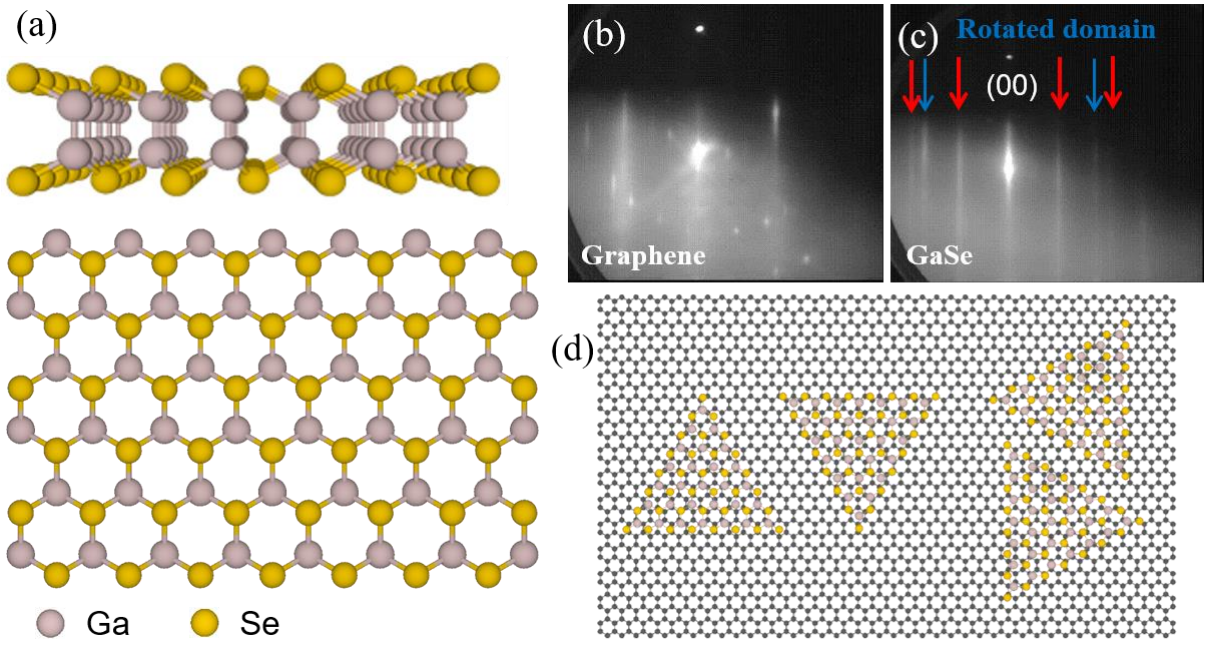

Figure 1: a) A schematic diagram of the side view and top view of hexagonal structure of GaSe (0001) (the grey spheres refer to Gallium atoms and the yellow spheres refer to the selenium atoms). b) RHEED pattern of graphene/6H-Si(0001) substrate: two streaky-line pattern attributed to graphene and interface layer and c) streaky-line pattern during the growth GaSe process along same electron-beam graphene azimuths in figure c) with the simultaneous presence in-plane of rotated GaSe domains (two streak-lines pattern: red (0°) and blue (30°) arrows); d) A scheme showing in-plane rotated GaSe domains on graphene in the nucleation regime (during the first tetra-atomic layer coverage of GaSe film). In the left-hand side, the triangular GaSe islands share a preferred lattice orientation with underlying lattice graphene layer with two twinned islands rotated by angle 180° between the edges of neighboring islands. On the right-hand side the GaSe islands are oriented ~ 30° angle apart.

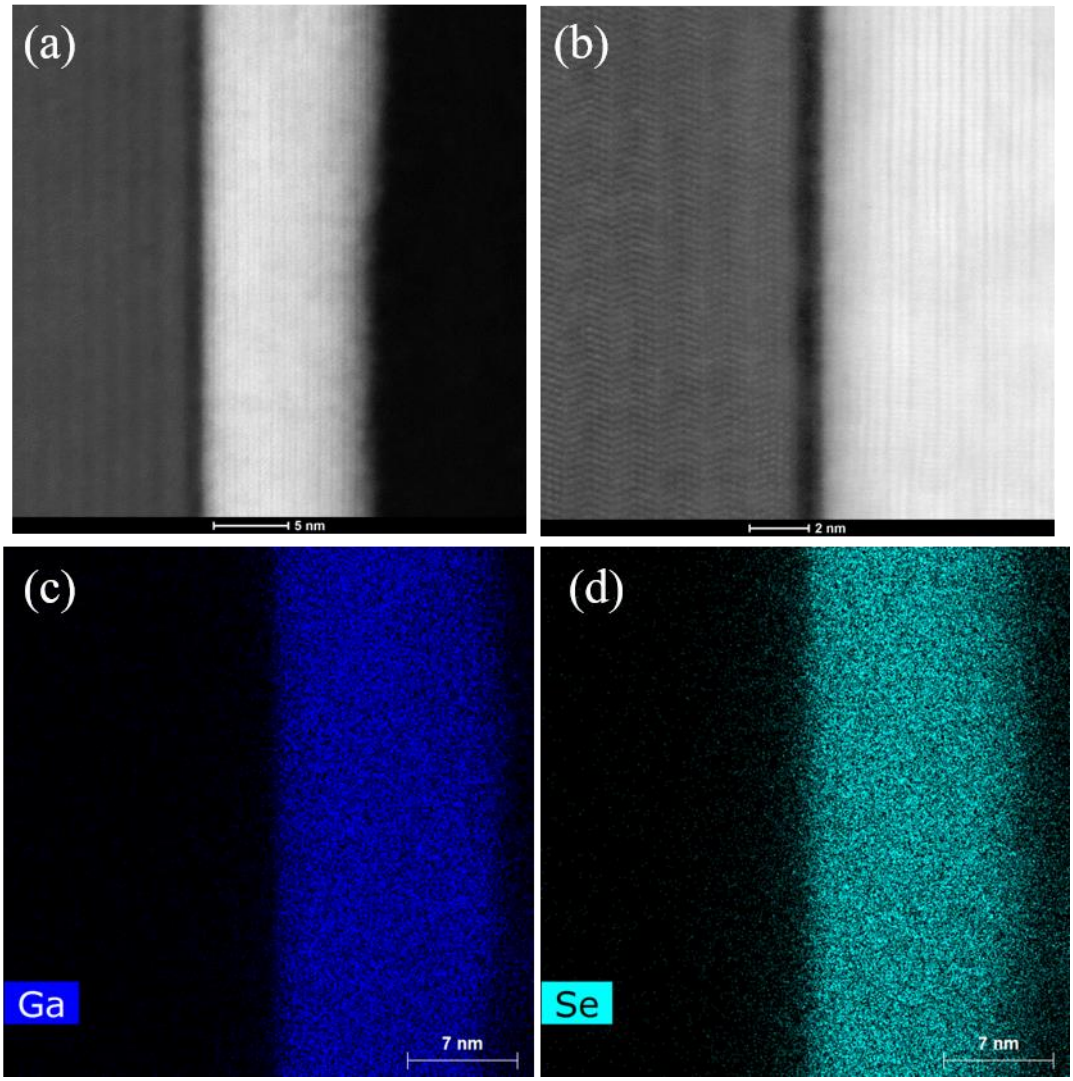

Figure 2: (a) and (b) Bright-field Scanning Transmission Electron Microscopy (STEM) image of GaSe/graphene heterostructure, high resolution STEM image place in the inset, the (c) (d) EDX elemental maps showing the spatial distribution of Ga and Se, respectively.

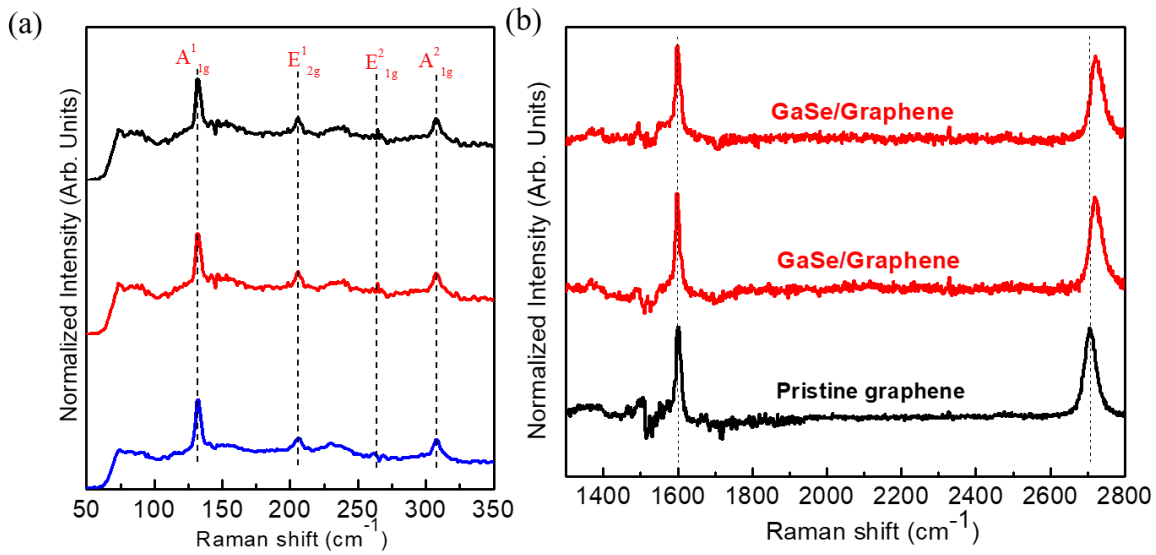

Figure 3: a) The characteristic peaks for different locations on GaSe grown on graphene, the spectra are exactly the same indicating substrate-independent growth with similar crystal quality owing to the vdW of 2D materials; b) Comparison of micro-Raman spectra taken on the pristine graphene (black color) and GaSe/graphene (red color) layers on different locations of the sample.

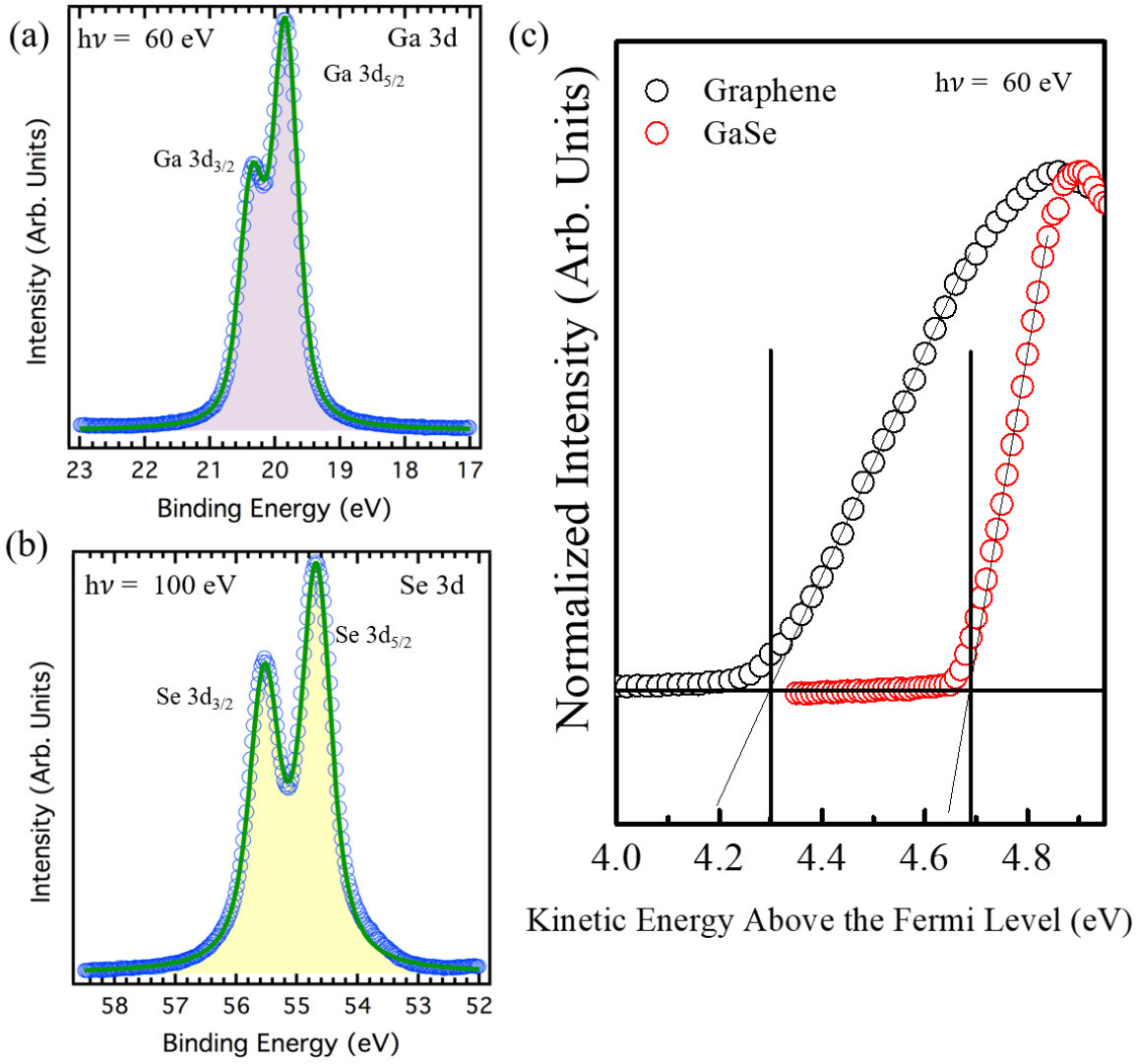

Figure 4: (a) and (b) Ga 3d and Se 3d core level XPS peaks of few layers GaSe grown on graphene. No reaction with the substrate is observed and the positions and line shapes of the Ga 3d and Se 3d peaks indicate Ga–Se bonding. (c) Secondary electron cut-off vs. kinetic energy referenced to the Fermi level to determine the work function of pristine graphene and GaSe/graphene heterostructure. The experimental data points are displayed as dots. The solid line is the envelope of fitted components.

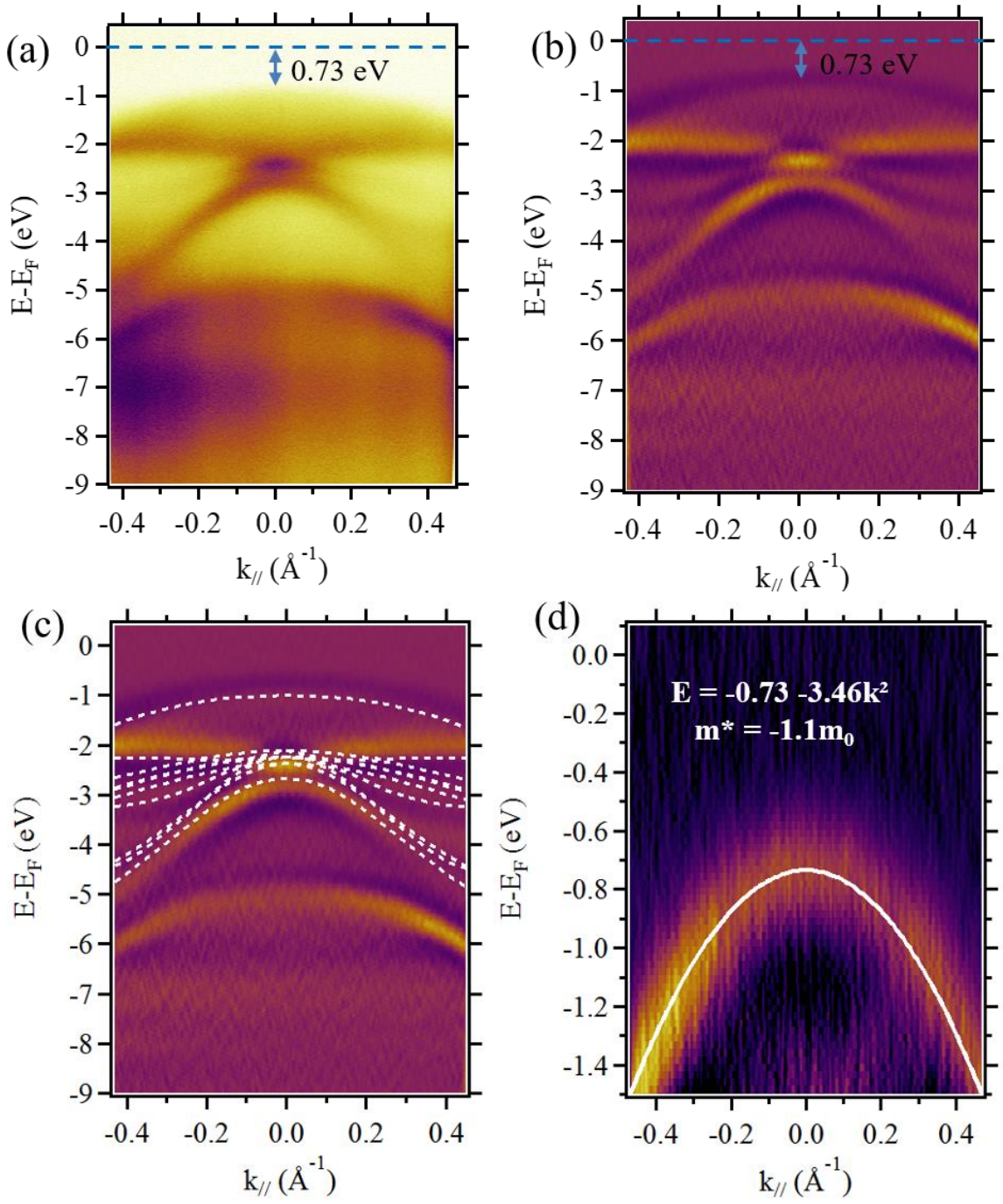

Figure 5: ARPES measurements of bulk GaSe on epitaxial graphene heterostructure: a) ARPES measurements of GaSe/graphene measured at hν = 60 eV along the ΓM direction of graphene first Brillouin zone, and b) The second derivative of the spectra a) exhibiting a better visibility of the bands. The Fermi level position is located at the zero of the binding energy (marked in blue dotted line). c) Comparison between the measured band structure and the theoretical calculation of bulk GaSe of X. Li et al[31] along the ΓM direction. d) The dispersion fitting used to determine the hole effective mass for GaSe defined along the ΓM direction.

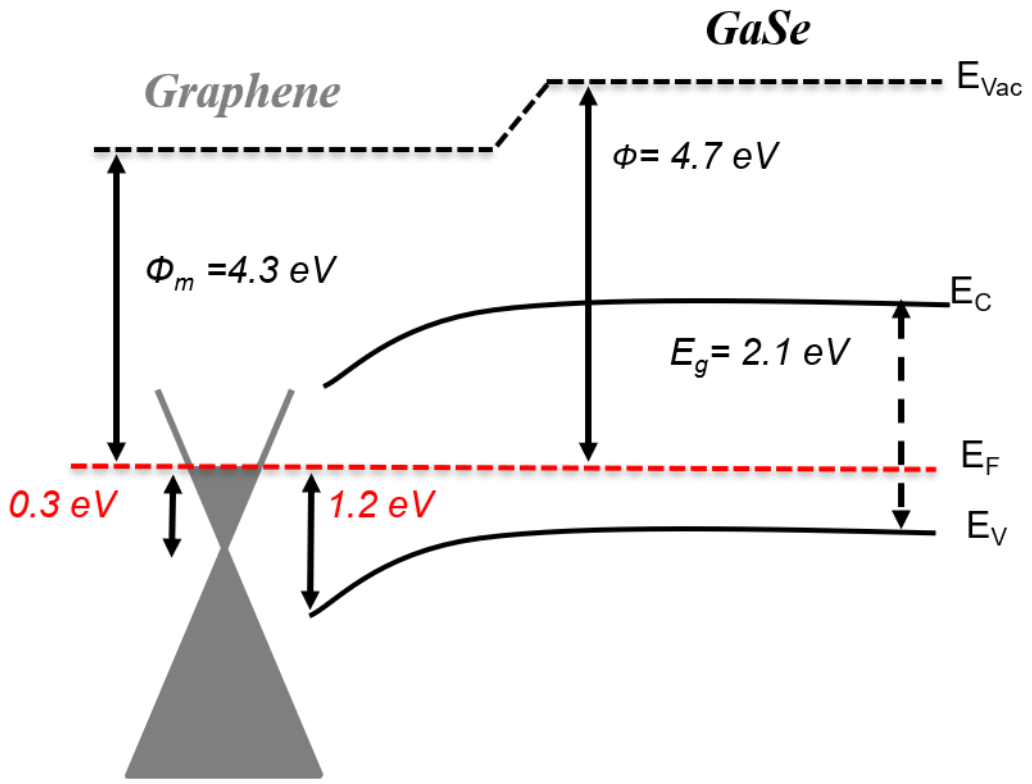

Figure 6: Schematic of the GaSe/Graphene band alignment diagram, as determined by XPS core level analysis. Φ and E_F denote the work function and the Fermi energy, respectively. E_g is the energy gap.

References:

(1) Geim, a K.; Grigorieva, I. V. *Nature* **2013**, *499* (7459), 419–425.

(2) Li, X.; Lin, M.-W.; Lin, J.; Huang, B.; Puretzky, A. A.; Ma, C.; Wang, K.; Zhou, W.; Pantelides, S. T.; Chi, M.; Kravchenko, I.; Fowlkes, J.; Rouleau, C. M.; Geohegan, D. B.; Xiao, K. *Sci. Adv.* **2016**, *2* (4), 2:e1501882.

(3) Li, X.; Basile, L.; Huang, B.; Ma, C.; Lee, J.; Vlassiouk, I. V; Puretzky, A. a; Lin, M.; Yoon, M.; Chi, M.; Idrobo, J. C.; Rouleau, C. M.; Sumpter, B. G.; Geohegan, D. B.; Xiao, K. *ACS Nano* **2015**, *9* (8), 8078–8088.

(4) Wu, C. H.; Yang, C. S.; Wang, Y. C.; Huang, H. J.; Ho, Y. T.; Wei, L. L.; Chang, E. Y. *Phys. Status Solidi Appl. Mater. Sci.* **2015**, *212* (10), 2201–2204.

(5) Hu, P.; Wen, Z.; Wang, L.; Tan, P.; Xiao, K. *ACS Nano* **2012**, *6* (7), 5988–5994.

(6) Bhimanapati, G. R.; Lin, Z.; Meunier, V.; Jung, Y.; Cha, J.; Das, S.; Xiao, D.; Son, Y.; Strano, M. S.; Cooper, V. R.; Liang, L.; Louie, S. G.; Ringe, E.; Zhou, W.; Kim, S. S.; Naik, R. R.; Sumpter, B. G.; Terrones, H.; Xia, F.; Wang, Y.; Zhu, J.; Akinwande, D.; Alem, N.; Schuller, J. A.; Schaak, R. E.; Terrones, M.; Robinson, J. A. *ACS Nano* **2015**, *9* (12), 11509–11539.

(7) Fang, H.; Battaglia, C.; Carraro, C.; Nemsak, S.; Ozdol, B.; Kang, J. S.; Bechtel, H. a; Desai, S. B.; Kronast, F.; Unal, A. a; Conti, G.; Conlon, C.; Palsson, G. K.; Martin, M. C.; Minor, A. M.; Fadley, C. S.; Yablonovitch, E.; Maboudian, R.; Javey, A. *Proc. Natl. Acad. Sci. U. S. A.* **2014**, *111* (17), 6198–6202.

(8) Rudolph, R.; Pettenkofer, C.; Bostwick, A. A.; Adams, J. A.; Ohuchi, F.; Olmstead, M. A.; Jaeckel, B.; Klein, A.; Jaegermann, W. *New J. Phys.* **2005**, *7*, 108.

(9) Pierucci, D.; Henck, H.; Avila, J.; Balan, A.; Naylor, C. H.; Dappe, Y. J.; Silly, M. G.; Sirotti, F.; Johnson, A. T. C.; M.C.Asensio; Ouerghi, A. *Nano Lett.* **2016**, *16*, 4054–4061.

(10) Fernelius, N. C. *Prog. Cryst. Growth Charact. Mater.* **1994**, *28* (4), 275–353.

(11) Cingolani, R.; Ferrara, M.; Lugara, M. *Phys. Scr.* **1988**, *583*, 583–586.

(12) Capozzi, V.; Montagna, M. *Phys. Rev. B* **1989**, *40* (5), 3182–3190.

(13) Huang, H.; Wang, P.; Gao, Y.; Wang, X.; Lin, T.; Wang, J.; Liao, L.; Sun, J.; Meng, X.; Huang, Z.;

Chen, X.; Chu, J. *Appl. Phys. Lett.* **2015**, *107* (14), 1–5.
(14) Lu, R.; Liu, J.; Luo, H.; Chikan, V.; Wu, J. Z. *Nat. Publ. Gr.* **2016**, 1–7.
(15) Shi, W.; Ding, Y. J. *Opt. Lett.* **2002**, *27* (16), 1454–1456.
(16) Allakhverdiev, K. R.; Yetis, M. Ö.; Özbek, S.; Baykara, T. K.; Salaev, E. Y. *Laser Phys.* **2009**, *19* (5), 1092–1104.
(17) Gillan, E. G.; Barron, A. R. **1997**, *4756* (12), 3037–3048.
(18) Mahjouri-samani, M.; Gresback, R.; Tian, M.; Wang, K.; Puretzky, A. A.; Rouleau, C. M.; Eres, G.; Ivanov, I. N.; Xiao, K.; Mcguire, M. A.; Duscher, G.; Geohegan, D. B. **2014**, 1–7.
(19) Chegwidden, S. *J. Vac. Sci. Technol. A Vacuum, Surfaces, Film.* **1998**, *16* (4), 2376.
(20) Vinh, L. T.; Eddrief, M.; Mahan, J. E.; Vantomme, A.; Song, J. H.; Nicolet, M.-A. *J. Appl. Phys.* **1997**, *81* (11), 7289.
(21) Yuan, X.; Tang, L.; Liu, S.; Wang, P.; Chen, Z.; Zhang, C.; Liu, Y.; Wang, W.; Zou, Y.; Liu, C.; Guo, N.; Zou, J.; Zhou, P.; Hu, W.; Xiu, F. *Nano Lett.* **2015**, *15* (5), 3571–3577.
(22) Lee, G.-H.; Lee, C.-H.; van der Zande, A. M.; Han, M.; Cui, X.; Arefe, G.; Nuckolls, C.; Heinz, T. F.; Hone, J.; Kim, P. *APL Mater.* **2014**, *2* (9), 92511.
(23) Pallecchi, E.; Lafont, F.; Cavaliere, V.; Schopfer, F.; Mailly, D.; Poirier, W.; Ouerghi, a. *Sci. Rep.* **2014**, *4*, 4558.
(24) Boutchich, M.; Arezki, H.; Alamarguy, D.; Ho, K.-I.; Sediri, H.; Güneş, F.; Alvarez, J.; Kleider, J. P.; Lai, C. S.; Ouerghi, a. *Appl. Phys. Lett.* **2014**, *105* (0001), 233111.
(25) Kuhn, a.; Chevy, a.; Chevalier, R. *Phys. Status Solidi* **1975**, *31*, 469–475.
(26) Plucinski, L.; Johnson, R.; Kowalski, B.; Kopalko, K.; Orlowski, B.; Kovalyuk, Z.; Lashkarev, G. *Phys. Rev. B* **2003**, *68*, 1–8.
(27) Liu, X.; Balla, I.; Bergeron, H.; Campbell, G. P.; Bedzyk, M. J.; Hersam, M. C. *ACS Nano* **2015**.
(28) Sediri, H.; Pierucci, D.; Hajlaoui, M.; Henck, H.; Patriarche, G.; Dappe, Y. J.; Yuan, S.; Toury, B.; Belkhou, R.; Silly, M. G.; Sirotti, F.; Boutchich, M.; Ouerghi, A. *Sci. Rep.* **2015**, *5*, 16465.
(29) Lei, S.; Ge, L.; Liu, Z.; Najmaei, S.; Shi, G.; You, G.; Lou, J.; Vajtai, R.; Ajayan, P. M. *Nano Lett.* **2013**, *13* (6), 2777–2781.
(30) Zhou, Y.; Zhou, Y.; Nie, Y.; Liu, Y.; Yan, K.; Hong, J.; Jin, C.; Yin, J.; Liu, Z.; Peng, H. *ACS Nano* **2014**, *8* (2), 1485–1490.
(31) Li, X.; Lin, M.-W.; Puretzky, A.; Idrobo, J. C.; Ma, C.; Chi, M.; Yoon, M.; Rouleau, C. M.; Kravchenko, I. I.; Geohegan, D. B.; Xiao, K. *Sci. Rep.* **2014**, *4*, 5497.
(32) Kim, W.; Li, C.; Chaves, F. A.; Jiménez, D.; Rodriguez, R. D.; Susoma, J.; Fenner, M. A.; Lipsanen, H.; Riikonen, J. *Adv. Mater.* **2016**, No. January 2016.
(33) Jnawali, G.; Rao, Y.; Beck, J. H.; Petrone, N.; Kymissis, I.; Hone, J.; Heinz, T. F. *ACS Nano* **2015**, *9* (7), 7175–7185.
(34) Das, A.; Pisana, S.; Chakraborty, B.; Piscanec, S.; Saha, S. K.; Waghmare, U. V; Novoselov, K. S.; Krishnamurthy, H. R.; Geim, A. K.; Ferrari, A. C.; SOOD, A. K. *Nat. Nanotechnol.* **2008**, *3* (4), 210–215.
(35) Yan, J.; Zhang, Y.; Kim, P.; Pinczuk, A. *Phys. Rev. Lett.* **2007**, *98* (16), 166802.
(36) Zhang, Y.; Tan, Y. W.; Stormer, H. L.; Kim, P. *Nature* **2005**, *438* (7065), 201–204.
(37) Pierucci, D.; Henck, H.; Naylor, C. H.; Sediri, H.; Lhuillier, E.; Balan, A.; Rault, J. E.; Dappe, Y. J.; Bertran, F.; Le Févre, P.; Johnson, A. T. C.; Ouerghi, A. *Sci. Rep.* **2016**, No. 6, 26656.
(38) Robin, A.; Lhuil, E.; Xu, X. Z.; Ithurria, S.; Aubin, H.; Ouerghi, A.; Dubertret, B. **2016**, 1–11.
(39) Lee, J. E.; Ahn, G.; Shim, J.; Lee, Y. S.; Ryu, S. *Nat. Commun.* **2012**, *3* (May), 1024.
(40) Ouerghi, a; Kahouli, a; Lucot, D.; Portail, M.; Travers, L.; Gierak, J.; Penuelas, J.; Jegou, P.; Shukla, a; Chassagne, T.; Zielinski, M. *Appl. Phys. Lett.* **2010**, *96* (19), 191910.
(41) Amokrane, A; Sebenne, C; Eddrief, M. *Surf. Sci.* **1998**, *124*, 619–625.
(42) Lang, O.; Klein, A.; Pettenkofer, C.; Jaegermann, W.; Chevy, A. *J. Appl. Phys.* **1996**, *80* (1996), 3817–3821.
(43) Iwakuro, H.; Ichimura, S. *Jpn. J. Appl. Phys.* **1982**, *21* (1 R), 94–99.
(44) Brumme, T.; Calandra, M.; Mauri, F. *Phys. Rev. B* **2015**, *91* (15), 155436.
(45) Zhang, Y.; Chang, T.-R.; Zhou, B.; Cui, Y.-T.; Yan, H.; Liu, Z.; Schmitt, F.; Lee, J.; Moore, R.; Chen, Y.; Lin, H.; Jeng, H.-T.; Mo, S.-K.; Hussain, Z.; Bansil, A.; Shen, Z.-X. *Nat. Nanotechnol.* **2014**, *9* (2), 111–115.
(46) Do, D. T.; Mahanti, S. D.; Lai, C. W. *Nat. Publ. Gr.* **2015**, 1–9.
(47) Lince, J. R.; Carr??, D. J.; Fleischauer, P. D. *Phys. Rev. B* **1987**, *36* (3), 1647–1656.
(48) Ghalouci, L.; Benbahi, B.; Hiadsi, S.; Abidri, B.; Vergoten, G.; Ghalouci, F. *Comput. Mater. Sci.* **2013**, *67*, 73–82.
(49) Del Pozo-Zamudio, O.; Schwarz, S.; Klein, J.; Schofield, R. C.; Chekhovich, E. a.; Ceylan, O.; Margapoti, E.; Dmitriev, a. I.; Lashkarev, G. V.; Borisenko, D. N.; Kolesnikov, N. N.; Finley, J. J.;

Tartakovskii, a. I. *arXiv* **2015**, 1–6.
(50) Pozo-Zamudio, O. Del; Schwarz, S.; Sich, M.; Akimov, I. A.; Bayer, M.; Schofield, R. C.; Chekhovich, E. A.; Robinson, B. J.; Kay, N. D.; Kolosov, O. V; A I Dmitriev; Lashkarev, G. V; Borisenko, D. N.; Kolesnikov, N. N.; Tartakovskii, A. I. *2D Mater.* **2015**, *2* (3), 035010.
(51) Yu, Y.-J.; Zhao, Y.; Ryu, S.; Brus, L. E.; Kim, K. S.; Kim, P. *Nano Lett.* **2009**, *9* (10), 3430–3434.
(52) Roldan, R.; Castellanos-Gomez, A.; Capelluti, E.; Guinea, F. *J. Phys. Condens. Matter* **2015**, *27*, 313201.
(53) Pierucci, D.; Sediri, H.; Hajlaoui, M.; Velez-Fort, E.; Dappe, Y. J.; Silly, M. G.; Belkhou, R.; Shukla, A.; Sirotti, F.; Gogneau, N.; Ouerghi, A. *Nano Res.* **2015**, *8* (3), 1026–1037.
(54) Penuelas, J.; Ouerghi, a.; Lucot, D.; David, C.; Gierak, J.; Estrade-Szwarckopf, H.; Andreazza-Vignolle, C. *Phys. Rev. B* **2009**, *79* (3), 033408.